

Cluster Simulations of Loop Models on Planar Lattices

Youjin Deng ¹ *, Wenan Guo ², Timothy M. Garoni ¹, Alan D. Sokal ¹, Henk W.J. Blöte ^{3,4}

¹*Department of Physics, New York University, New York NY 10003, USA*

²*Physics Department, Beijing Normal University, Beijing 100875, China*

³*Faculty of Applied Sciences, Delft University of Technology, P.O. Box 5046, 2600 GA Delft, The Netherlands*

⁴*Lorentz Institute, Leiden University, P.O. Box 9506, 2300 RA Leiden, The Netherlands*

(December 2, 2024)

Abstract

Making use of the duality relation of the Ising model, we develop cluster algorithms for several loop models on planar lattices. We then investigate the $O(n)$ model on the honeycomb lattice and face- and corner-cubic models on the square lattice. Several new physical phenomena are observed. For instance, critical exponents, which have not been reported for the $O(n)$ model in literature, are determined; both ‘ferromagnetic’ and ‘antiferromagnetic’ phase transitions are located for the cubic models. Dynamical behavior is also studied. It is shown that, for $1 < n \leq 2$, our cluster algorithms *hardly* suffer from critical slowing down.

Typeset using REVTEX

*Email: yd10@nyu.edu

A celebrated event in Monte Carlo studies of statistical systems was the invention of the Swendsen-Wang (SW) cluster Monte Carlo method in 1987 [1]. This algorithm has then been widely acclaimed for its ability to suppress critical slowing down. The SW algorithm is formulated with the help of the random-cluster representation [2] of the Potts model, which expresses the Potts partition sum in terms of *independent* clusters of spins. Thus, an arbitrary spin state can be assigned to each cluster, and *nontrivial global* updates are allowed.

Since then, the SW method and its generalizations have had a large impact on the study of critical phenomena in lattice spin models. The Wolff algorithm [3], a single-cluster version of the SW method, is now widely used because of its simplicity and further improves efficiency. An algorithm of Chayes and Machta [4] enables cluster simulations of the q -state random-cluster model with real value $q \geq 1$. The invaded cluster method [5] and the probability-changing cluster algorithm [6] are found to be useful in locating critical points of various models. Luijten and Blöte [7] introduced a cluster method that is particularly efficient for systems with long-rang interactions [8]. A cluster method [9] was found for the quantum Ising model in transverse fields.

However, efficient cluster simulations still remain as a long-standing problem for another important class of models in statistical physics—the loop model.

Loop models are graphical models defined by drawing *closed* loops along the bonds of the underlying lattice. The loops may come in n different colors. No two loops can share a bond, while sharing a vertex is generally allowed. Explicitly, the bond configurations are such that each vertex is incident to an even number—possibly zero—of bonds of each color. Namely, they are Eulerian. Each loop configuration is assigned a ‘weight’ that depends on participating vertices of each type.

Loop models appear quite naturally as representations (often approximate) of various statistical-mechanical models. These include the Ising model, the Potts model, $O(n)$ spin models, the n -component Ashkin-Teller model, 1-D quantum spin models, a supersymmetric spin chain, the q -coloring problem, and polymer models.

A considerable amount of work has been carried out on the subject. Exact results have been obtained for some special cases like the the loop model on the honeycomb lattice [10,11]. Numerical techniques, like transfer-matrix calculations [12], have also been employed. Nevertheless, many open questions still exist. The nature of phase transitions is still unclear for the honeycomb loop model with sufficient dilutions; there is no consensus yet about the phase diagrams of loop models with self-interactions, such as face- and corner-cubic models on the square lattice. For some recent publications, see Refs. [13–16].

We start with an $O(n)$ spin model

$$\mathcal{Z}(x, n) = \text{Tr} \prod_{\langle ij \rangle} (1 + nx \vec{S}_i \cdot \vec{S}_j), \quad (1)$$

where $\vec{S} \in \mathbb{R}^n$, $|\vec{S}| = 1$, x is a measure of the inverse temperature, and Tr denotes normalized integration over all possible spin configurations. For $n \neq 1$, model (1) is not equivalent to the conventional $O(n)$ spin model, but it is expected that they belong to the same universality class. The corresponding loop model of Eq. (1) is readily obtained along the line of a typical “high-temperature” expansion. On lattices of maximum degree 3, it reduces to a gas of nonintersecting loops

$$\mathcal{Z}_{O(n)}(x, n) = \sum_{\mathcal{G}: \text{Eu.}} x^{b(\mathcal{G})} n^{\ell(\mathcal{G})}, \quad (2)$$

where the sum is over all Eulerian (Eu.) subgraphs \mathcal{G} . Symbol b is the total number of occupied bonds, and ℓ is the number of loops. Note that n can now be considered as a continuous parameter.

On the honeycomb lattice, the loop model (2) can be further mapped onto the Kagomé 6-vertex model and the Coulomb gas, and therefore many exact results are available. The critical frontier for $n \leq 2$ was located [11] at $x_c(n) = (2 + \sqrt{2 - n})^{-1/2}$. It was also observed [11] that a *critical* $O(n)$ model corresponds with a *tricritical* $q = n^2$ -state Potts model. From conformal field theory and Coulomb gas theory, exact values of critical exponents are predicted as

$$y_{t0} = \frac{3g - 6}{g}, \quad y_{t1} = \frac{4g - 16}{g}, \quad y_{h0} = \frac{(g + 6)(g + 2)}{8g}, \quad (3)$$

where the Coulomb-gas coupling g is related to n as $g = 4 + (4/\pi) \arccos[n/2]$, while y_{t0} and y_{t1} are respectively the leading and the subleading thermal exponents, and y_{h0} is the leading magnetic exponent. The leading exponents y_{t0} and y_{h0} do not occur in the thermodynamic singularities of models with $O(n)$ universality, but they do govern the singularities of the closely related tricritical Potts models [11].

A discrete face-cubic model is defined by restricting the spins to $2n$ orientations along n Cartesian axes: $\mathcal{Z} = \text{Tr} \prod_{\langle ij \rangle} \left[1 + xn \left(u_i^{(1)} u_j^{(1)} + \cdots + u_i^{(n)} u_j^{(n)} \right) \right]$, where $u_i^{(k)} = 0, \pm 1$, and for a given site i exactly one of $u_i^{(k)}$ ($k = 1, 2, \dots, n$) has a non-zero value. The variables u_k are thus components of unit vectors that point from the center to the faces of an n -dimensional hypercube. Its cluster representation is

$$\mathcal{Z}_{Fc}(x, n) = \sum_{\mathcal{G}:\text{Eu.}} x^{b(\mathcal{G})} n^{f(\mathcal{G})}, \quad (4)$$

with f being the total number of *loops*—i.e., the cyclomatic number of \mathcal{G} . The number f is the minimum number of bonds that one must remove in order for the remaining clusters to be tree-like.

The corner-cubic model is defined by $\mathcal{Z} = \text{Tr} \prod_{\langle ij \rangle} \left[1 + x \left(s_i^{(1)} s_j^{(1)} + \cdots + s_i^{(n)} s_j^{(n)} \right) \right]$, where $s_i^{(k)} = \pm 1$ are the components of a vector pointing from the center to the corner of a n -dimensional hypercube. We assign color k for each Ising variable $s^{(k)}$, and the resulting loop model becomes

$$\mathcal{Z}_{Cc}(x, n) = \sum_{\mathcal{G}^{(1)}:\text{Eu.}} \cdots \sum_{\mathcal{G}^{(n)}:\text{Eu.}} x^{b(\mathcal{G})}, \quad (5)$$

where $\mathcal{G}^{(k)}$ consists of bonds in color k . No two subgraphs share a common edge. Unlike in Eqs. (2) and (4), n is here restricted to integer values.

For $n = 1$, the above models all reduce to the Ising model with couplings given by $\tanh K = x$. On a planar lattice \mathcal{L} , such a loop model also represents the low-temperature graphs of an Ising model on the dual lattice \mathcal{D} with $e^{-2K} = x$. A low-temperature graph on \mathcal{L} consists of those edges separating associated pairs of neighboring Ising spins on \mathcal{D} .

A loop graph on \mathcal{L} corresponds to two Ising spin configurations on \mathcal{D} , which are related by flipping all the spins. This is valid for *any* loop model on planar lattices. We thus explore the possibility to simulate loop models by flipping the spins on \mathcal{D} .

For the $O(n)$ model (2) with $n \geq 1$, we first randomly assign color variables to each loop: color 1 with probability $p = 1/n$, and color 2 with $p = 1 - 1/n$. Next we introduce an auxiliary variable η for each edge on \mathcal{L} . If the edge is covered by a loop, η takes the value of its color; otherwise, $\eta = 0$. Accordingly, the edge set $E_{\mathcal{L}}$ of \mathcal{L} splits into three subsets $E_{\mathcal{L}}^{(\eta)}$ with $\eta = 0, 1$ and 2 . The color variables in sets $E_{\mathcal{L}}^{(1)}$ and $E_{\mathcal{L}}^{(2)}$ can be updated independently. The Ising spins separated by edges of color 0 and 1 can be simulated by existing algorithms for the Ising model. Color 2 can be simply chosen to remain unaffected and the edges of \mathcal{D} crossing these loops are thus covered by a rigid bond, as accounted for by the following operations [*Algorithm 1*]:

1. For each loop, set $\eta = 1$ with probability $p = 1/n$ and $\eta = 2$ with $p = 1 - 1/n$. The edge variables on these loops take that value of η , and the remaining edge variables on \mathcal{L} take $\eta = 0$.
2. Let each edge of the dual lattice \mathcal{D} take the value η of the corresponding edge on \mathcal{L} . If $\eta = 0$, place a bond with probability $p = 1 - x$; if $\eta = 1$, place no bond ($p = 0$); if $\eta = 2$, place a bond ($p = 1$).
3. Form clusters on \mathcal{D} from sites connected by bonds. Randomly flip the Ising spins on each cluster with probability $1/2$. Note that a cluster may contain both ± 1 Ising spins.

We remark that Step 2 requires $x \leq 1$, but it is straightforward to generalize the algorithm to the case $x > 1$, which corresponds to antiferromagnetic coupling $e^{-2K} = x > 1$ for the dual Ising spins.

Analogous procedures can be applied to simulate the face-cubic model (4) with $n \geq 1$. First, one identifies Ising clusters on the dual lattice \mathcal{D} by connecting all spins except those intersecting a loop of Eq. (4). The loops separate Ising clusters of different sign. One then

sets the auxiliary variable η for each site on \mathcal{D} . A cluster Monte Carlo step then reads [Algorithm 2]:

1. Form Ising clusters on \mathcal{D} . To each cluster, set $\eta = 1$ with probability $p = 1/n$ or $\eta = 2$ with $p = 1 - 1/n$.
2. For each edge $\langle ij \rangle_{\mathcal{D}}$, place a bond with probability $p = 1 - x$ if $s_i = s_j$ and $\eta_i = \eta_j = 1$, $p = 0$ if $s_i \neq s_j$ and $\eta_i = \eta_j = 1$, and $p = 1$ if $\eta_i = 2$ or $\eta_j = 2$.
3. Same as Step 3 in Algorithm 1.

Before describing the cluster algorithm for the corner-cubic model of Eq. (5), we first consider the restricted corner-cubic model of Ref. [10] in which neighboring spins may differ in at most one component. It can be reformulated as a n -component Ashkin-Teller (AT) model [17]. On every vertex i , place n Ising spins $s_i^{(k)}$ with color $k = 1, 2, \dots, n$. The Hamiltonian reads

$$\mathcal{H} = - \sum_{k=1}^n \sum_{\langle i,j \rangle} s_i^{(k)} s_j^{(k)} (J_2 + J_4 \sum_{l>k} s_i^{(l)} s_j^{(l)}) , \quad (6)$$

with coupling constants $J_2 \rightarrow \infty$ and $J_4 \rightarrow -\infty$, while $J \equiv J_2 + (N-1)J_4$ is finite. Let r denote the number of colors whose spin pairs are different on edge $\langle ij \rangle$: $s_i^{(k)} \neq s_j^{(k)}$. The statistical weight of edge $\langle ij \rangle$ is, relative to case $r = 0$, given by Table I. Thus, for any edge $\langle ij \rangle$ there is *at most* one pair of unequal spins of the same color.

We refer to this infinite-coupling AT model (6) as the IAT model. This model, and the restricted corner-cubic model, are dual to the corner-cubic model (5) [17] with the relation $x = e^{-2J}$.

For a given color of Ising variable $s^{(k)}$ in the IAT model, the effective Hamiltonian, conditioned on the other spin configurations $s^{(l)} (l \neq k)$, has nearest-neighbor pair couplings only, which read $J_{\text{eff}} = J_2 + J_4 \sum_{l \neq k} s_i^{(l)} s_j^{(l)}$. Thus, when all spin pairs $s_i^{(l)}$ and $s_j^{(l)}$ are equal for $l \neq k$, then the coupling $J_{\text{eff}} = J_2 + (n-1)J_4 \equiv J$ is finite. Otherwise, for r unequal pairs with $l \neq k$, one has $J_{\text{eff}} = J - 2rJ_4 \rightarrow \infty$.

On this basis, together with the symmetry between different colors of Ising spins, one can construct the following Monte Carlo step [*Algorithm 3*]:

1. Random Interchange.

- (a) Randomly choose two colors of spins $s^{(k)}$ and $s^{(l)}$ (defined on \mathcal{D}), and calculate product $s = s^{(k)} \cdot s^{(l)}$ for every vertex.
- (b) Construct Ising clusters for the product spin s . To each Ising cluster, randomly assign spin state $s^{(k)} = +1$ or -1 with probability $1/2$, and let $s^{(l)} = s \cdot s^{(k)}$.

2. Simulation for spin $s^{(k)}$.

- (a) Place bonds. For every edge $\langle ij \rangle$ on \mathcal{D} , an occupied bond is placed with probability: $p = 1 - x$ if $s_i^{(k)} = s_j^{(k)}$ and $s_i^{(r)} = s_j^{(r)}$ for all $r \neq k$, $p = 0$ if $s_i^{(k)} \neq s_j^{(k)}$, and $p = 1$ if $s_i^{(k)} = s_j^{(k)}$ and $s_i^{(r)} \neq s_j^{(r)}$ for any one $r \neq k$.
- (b) Identify clusters based on the occupied bonds, and flip spins $s^{(k)}$ to each cluster with probability $p = 1/2$.

While step 1 updates the spin variables $s^{(k)}$ and $s^{(l)}$, it does not change the total energy of the system. Nevertheless, as we shall see, this step suppresses dynamical critical slowing down.

The known properties of Ising-like random clusters indicate that these cluster algorithms are valid. We skip further theoretical justification and illustrate the validity and the efficiency of the algorithms by the following applications.

We first investigate the $O(n)$ model (2) on the honeycomb lattice. The corresponding Ising model is defined on the $L \times L$ triangular lattice. The lattice size L took 20 values in range $6 \leq L \leq 1024$. Periodic boundary conditions were applied.

The above three algorithms are actually all valid for the honeycomb $O(n)$ model (2) (Algorithm 3 works only for integer $n \geq 2$). It can be shown that their efficiency differs only by a constant factor. We simply chose Algorithm 1.

Samples were taken after every Monte Carlo step. The sampled quantities include the specific-heat-like quantity $C = (\langle b^2 \rangle - \langle b \rangle^2)/L^2$ and susceptibility $\chi = L^2\langle m^2 \rangle$, where b is the bond number in Eq. (2) and m is the Ising magnetization density. Moreover, in each sampling step, we neglect the colors of loops involved in the simulations, and reassign the color of each loop to be α or β with probability 1/2. Then, we performed a similar sampling for the number $b^{(\alpha)}$ of loops of color α , and the magnetization $m^{(\alpha)}$ of the triangular lattice Ising configuration dual to the color- α loops. We thus sampled $C^{(\alpha)} = (\langle b^{(\alpha) 2} \rangle - \langle b^{(\alpha)} \rangle^2)/L^2$ and $\chi^{(\alpha)} = L^2\langle m^{(\alpha) 2} \rangle$.

We performed such simulations for $n = 1.25, 1.50, 1.75$, and 2.00 . The results for the critical points are in satisfactory agreement with the exact predictions. We observed that the finite-size scaling behavior of quantities $C^{(\alpha)}$ and χ , C , and $\chi^{(\alpha)}$ is governed by exponents y_{t0} , y_{t1} , and y_{h0} in Eq. (3), respectively. The numerical results are shown in Table II. To our knowledge, numerical determination of exponents y_{t0} and y_{h0} has not yet been reported in $O(n)$ models.

We have also determined the integrated autocorrelation time τ for susceptibilities χ and $\chi^{(\alpha)}$, and for the bond numbers b and $b^{(\alpha)}$. It is found that for $2 \geq n > 1$ critical slowing down *hardly* exists. The τ data for $n = 2$ are shown in Fig. 1, which strongly suggests that the dynamic exponent z is zero for $n = 2$.

We have also simulated the critical $O(2)$ model by Algorithm 3 but without Step 1. The dynamic exponent was determined as $z = 1.17(1)$, satisfying the Li-Sokal bound [18] due to exponent y_{t0} : $z \geq 2y_{t0} - 2 = 1$. For $L = 256$, the integrated correlation time is $\tau = 996(16)$ for quantity $\chi^{(1)}$. Compared with Fig. 1, this justifies Step 1 of Algorithm 3 since it suppresses critical slowing down. Apparently, the Li-Sokal bound $z \geq 1$ is not satisfied by Algorithm 3. This is because the symmetry between different colors of Ising spins is used in Step 1.

For loop models on lattices where loop interactions are allowed, the phase diagrams for $n > 2$ are largely unexplored.

We investigated models (4) and (5) on the square lattice by Algorithms 2 and 3, respectively. In both models, two distinct phase transitions are found, which correspond to the “ferromagnetic” and “antiferromagnetic” transitions in terms of the Ising spins on the dual lattice \mathcal{D} . They are shown in Fig. 2 for model (4), for several values of $n \geq 1$. The results for the critical points agree accurately with those given in Ref. [19] for $n \leq 2$. Our data show that the lines of phase transitions extend to $n > 2$, but in the unphysical range $x > 1/n$ of the spin model.

In short, we have developed efficient cluster algorithms and applied it to several loop models. These methods may play a significant role in the study of open problems in the physics of loop models. Finally, we mention that single-cluster (Wolff-like) versions of Algorithms 1-3 can be constructed and that Algorithm 3 can be generalized for the corner-cubic model with real value $n = k/2^l (n \geq 1)$, where k and l are integers.

Acknowledgment: This research was supported by U.S. National Science Foundation Grant No. PHYS-0424082, by the National Science Foundation of China under Grant No. 10105001, and by the FOM (“Fundamenteel Onderzoek der Materie”) Foundation of the Netherlands.

REFERENCES

- [1] R.H. Swendsen and J.-S. Wang, Phys. Rev. Lett. **58**, 86 (1987).
- [2] P.W. Kasteleyn and C.M., J. Phys. Soc. Jpn. Suppl. **26s**, 11 (1969).
- [3] U. Wolff, Phys. Rev. Lett. **62**, 361 (1989).
- [4] L. Chayes and J. Machta, Physica A **254**, 477 (1998); **239**, 542 (1997).
- [5] J. Machta, Y. S. Choi, A. Lucke, T. Schweizer, and L. M. Chayes, Phys. Rev. Lett. **75**, 2792 (1996).
- [6] Y. Tomita and Y. Okabe, Phys. Rev. Lett. **86**, 572 (2001).
- [7] E. Luijten and H.W.J. Blöte, Int. J. Mod. Phys. C **6**, 359 (1995).
- [8] E. Luijten and H.W.J. Blöte, Phys. Rev. Lett. **76**, 1557 (1996); **89**, 025703 (2002).
- [9] Y. Deng and H.W.J. Blöte, Phys. Rev. Lett. **88**, 190602 (2002); H.W.J. Blöte and Y. Deng, Phys. Rev. E **66**, 066110 (2002).
- [10] E. Domany, D. Mukamel, B. Nienhuis, and A. Schwimmer, Nucl. Phys. B **190**, 279 (1981).
- [11] B. Nienhuis, Phys. Rev. Lett. **49**, 1062 (1982).
- [12] W. Guo, H.W.J. Blöte, and F.Y. Wu, Phys. Rev. Lett. **85**, 3874 (2000).
- [13] L. Chayes, L.P. Pryadko, and K. Shtengel, Nucl. Phys. B **570**, 590 (2000).
- [14] J.L. Jacobsen, N. Read, and H. Saleur, Phys. Rev. Lett. **90**, 090601 (2003).
- [15] W. Janke and A.M.J. Schakel, Phys. Rev. Lett. **95**, 135792 (2005).
- [16] W. Guo, B. Nienhuis, and H.W.J. Blöte, Phys. Rev. Lett. **96**, 045704 (2006).
- [17] Y. Deng, W. Guo, and H.W.J. Blöte, arXiv: con-mat/0605165.
- [18] X.J. Li and A.D. Sokal, Phys. Rev. Lett. **63**, 827 (1989).

[19] W. Guo, X. Qian, H.W.J. Blöte, and F.Y. Wu, Phys. Rev. E **73**, 026104 (2006).

FIGURES

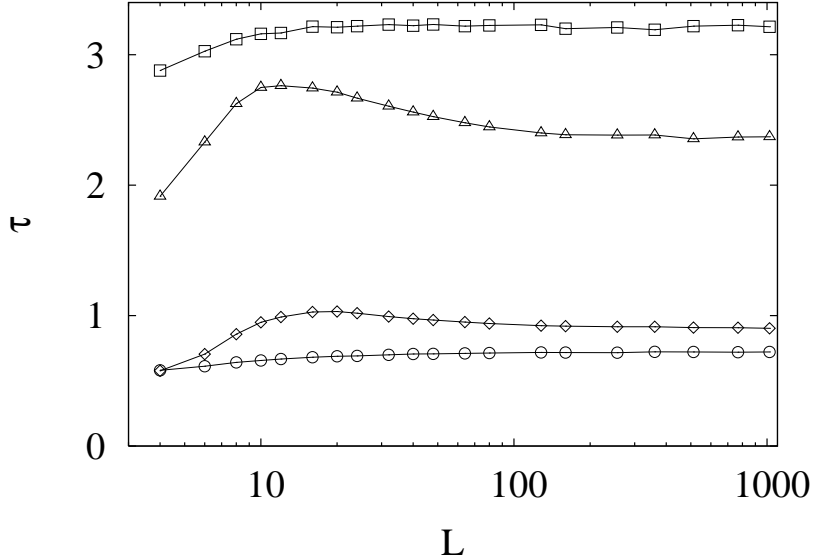


FIG. 1. Integrated autocorrelation time τ for the O(2) model versus finite size L . The data points \square , \circ , \triangle , and \diamond apply to the quantities χ , $\chi^{(1)}$, b , and $b^{(1)}$, respectively. Statistical error margins are about the size of the data points.

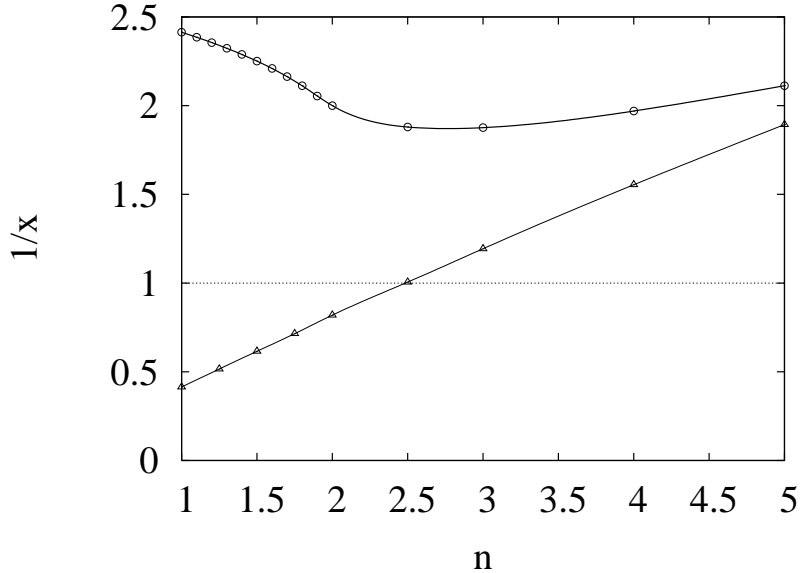


FIG. 2. Location of the ferro- and antiferromagnetic phase transitions of the face-cubic model versus n . The data points \circ and \triangle apply to the ferromagnetic and the “antiferromagnetic” phase transition respectively.

TABLES

N		y_{t0}	y_{t1}	y_{h0}
1.25	Exact	1.8327	0.8873	1.9343
	Num.	1.8327(2)	0.887(2)	1.9342(2)
1.50	Exact	1.7805	0.7481	1.9198
	Num.	1.7801(4)	0.745(4)	1.9199(2)
1.75	Exact	1.7078	0.5542	1.9034
	Num.	1.7079(4)	0.54(1)	1.9032(2)
2.00	Exact	1.5	0	1.875
	Num.	1.5002(4)	0.1(2)	1.8751(1)

TABLE I. A comparison of the critical exponents determined by Monte Carlo simulations and those predicted by Eq. (3).

 TABLE II. Edge weights for model (6) for several r .

Configuration	Normalized weight
$r = 0$	1
$r = 1$	$e^{-2[J_2 + (N-1)J_4]} \equiv e^{-2J}$
$r \geq 2$	$e^{-2rJ} \cdot e^{r(r-1)J_4} \rightarrow 0$